Molecular Crystals and Liquid Crystals Science and Technology. Section A. Molecular Crystals and Liquid Crystals

Publication details, including instructions for authors and subscription information:
http://www.tandfonline.com/loi/gmcl19

# Spectroscopic and Crystallographic Study of Phase Transitions in Zn Bidimensional Complexes

M. Rey-lafon [a] , C. Lartigue-bourdeau [b] , Th. Maris [b] , M. Khechoubi [b] & N. B. Chanh [b]

[a] Laboratoire de Spectroscopie MoléCulaire et Cristalline-CNRS URA 124, Université Bordeaux, 1-33405, Talence, France

[b] Laboratoire de Cristallographie et de Physique Cristalline -CNRS ERS 133, Université Bordeaux, 1-33405, Talence, France

Version of record first published: 24 Sep 2006.

To cite this article: M. Rey-lafon , C. Lartigue-bourdeau , Th. Maris , M. Khechoubi & N. B. Chanh (1995): Spectroscopic and Crystallographic Study of Phase Transitions in Zn Bidimensional Complexes, Molecular Crystals and Liquid Crystals Science and Technology. Section A. Molecular Crystals and Liquid Crystals, 269:1, 55-73

To link to this article: http://dx.doi.org/10.1080/10587259508037321

*Mol. Cryst. Liq. Cryst.*, 1995, Vol. 269, pp. 55–73
Reprints available directly from the publisher
Photocopying permitted by license only





# Spectroscopic and Crystallographic Study of Phase Transitions in Zn Bidimensional Complexes

M. REY-LAFON

*Laboratoire de Spectroscopie Moléculaire et Cristalline-CNRS URA 124 Université Bordeaux I-33405-Talence (France)*

and

C. LARTIGUE-BOURDEAU, TH. MARIS, M. KHECHOUBI and N. B. CHANH

*Laboratoire de Cristallographie et de Physique Cristalline -CNRS ERS 133 Université Bordeaux I-33405-Talence (France)*

*(Received 19 September 1994; in final form 2 December 1994)*

The solid phases which appear when heating crystalline bis *n*-decyl and *n*-dodecyl ammonium tetrachlorozincates ($C_{10}Zn$ and $C_{12}Zn$ for short) were studied using differential scanning calorimetry, X-ray diffraction and infrared and Raman spectroscopies. The unit-cell parameters of the different phases were determined. For $C_{10}Zn$ as well as for $C_{12}Zn$, the room temperature stable phase is a well-ordered interdigitated layer structure with chains in all-trans conformation. A great mobility of the chains is observed when raising temperature within the phase, but the formation of specific sequences of bonds, mainly kinks $gt^{2n-1}g'$ and end gauche forms, abruptly occurs at the first transition temperature at the same time as the cell parameters change. The consecutive increase in the chain diameter induces a partial disinterdigitation. A second phase change at higher temperature leads to a highly disordered form in which only the inorganic matrix keeps a bidimensional crystallographic organization, before reaching the isotropic phase.

*Keywords: bilayered compounds, order-disorder phase transitions, molecular conformation, X-ray diffraction, calorimetry, vibrational analysis*

## ABBREVIATIONS

| | |
|---|---|
| $C_{10}Zn$ | $(C_{10}H_{21}NH_3)_2\ ZnCl_4$ |
| $C_{12}Zn$ | $(C_{12}H_{25}NH_3)_2\ ZnCl_4$ |
| RTP | room temperature phase |
| MTP | middle temperature phase |
| HTP | high temperature phase |
| LAM | longitudinal accoustic mode |
| ITP | intermediate temperature phase |

| | |
|---|---|
| DSC | differential scanning calorimetry |
| IR | infrared |
| g | gauche |
| t | trans |

## INTRODUCTION

Compounds of the general formula $(n\text{-}C_nH_{2n+1}NH_3)_2\,MCl_4$ ($C_n$ M, with M = Cd, Mn, Cu, Pb, Hg, Zn, Co) are characterized, in the low temperature solids which are structurally defined by ionic sheets constituted of macroanions M $Cl_4$, each of them sandwiched between two alkylammonium layers. When M = Zn, the ionic layers are formed of single $(ZnCl_4)^{--}$ tetrahedron dianions, each dianion being surrounded by six $NH_3^+$ groups. X-ray diffraction experiments showed that the alkyl chains are interdigitated when $n = 12, 14, 16$[1,2,3] (Figure 1). This structure is different from that of compounds with M = Cd, Mn, Pb where the mineral layers are constituted of corner sharing $MCl_6$ octahedra.[4] Numerous studies revealed that phase transitions in the latter derivatives are related to the cation dynamics (i.e. reorientational phenomena and cooperative conformational changes of alkyl chains). However the phase change sequence and the mechanism of the disordering process seem very dependent on the packing of the chains and the way they are bound to the inorganic matrix. Because of the structural differences from the other members of the family, it seems quite interesting to investigate the phase transitions of Zn derivatives in order to understand the microscopic aspect of their mechanism.

We choose to study $C_{12}Zn$ and $C_{10}Zn$, since the $C_{12}Zn$ structure has been published.[1] Additionally the dynamics of the decylammonium cations have been investigated in $C_{10}Cd$,[4,5] $C_{10}Mn$,[6,7] $C_{10}Cu$,[8,9] and *n*-decylammonium chloride $(C_{10}Cl)$[10], $C_{10}Zn$ molecular and crystalline structures are not known. Differential scanning calorimetric measurements on each compound evidenced the existence of one structural phase transition at 351 K for $C_{10}Zn$ and 360.5 K for $C_{12}Zn$ and another one near 436 K for both compounds which corresponds to an evolution to a highly disordered phase.[11] An additional phase change at 284 K was revealed by thermal analysis and proton nuclear magnetic resonance, when heating a virgin polycrystalline sample of $C_{10}Zn$,[12] however no structural difference was observed at this transition.

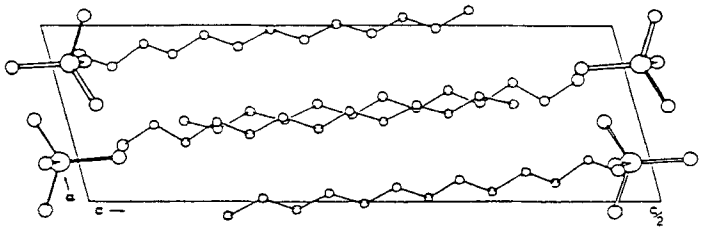


FIGURE 1 Molecular model of $(n\text{-}C_{12}H_{25}NH_3)_2\,ZnCl_4$ ($C_{12}Zn$ as short name). Projection along the *b* axis [1].

In order to determine the accurate temperature of phase transitions in our samples, we performed DSC experiments on $C_{10}Zn$ and $C_{12}Zn$ using low heating and cooling rates so as to avoid a temperature shift of the thermal signals. Then, the crystallographic aspect of the polymorphic behaviour was studied by X-ray diffraction experiments on powder samples. To obtain information on the chain conformation and its evolution in the different phases, we used vibrational infrared and Raman spectroscopies. All the measurements were performed at temperatures higher than 290 K.



## I. EXPERIMENTAL

*n*-alkylammonium chlorides were prepared by bubbling gaseous HCl through an ethanolic solution of the corresponding amine. $C_{10}Zn$ and $C_{12}Zn$ were then obtained by mixing ethanolic solutions of *n*-alkylammonium and Zn chloride in stoichiometric proportions. The products were purified by crystallization from ethanol.

Calorimetric investigations were carried out in the range 293–460 K with a Perkin-Elmer DSC Series 7. The powdered sample, about 3–6 mg was sealed in aluminium pans. The heating and cooling rates were $2\,K\,min^{-1}$. For each compound, two experiments were performed and the results averaged. The characteristics of each DSC peak were determined according to international convention by the "onset" temperature $T_0$ and the peak temperature $T_s$, and the corresponding enthalpic value was obtained from a signal treatment program. The enthalpic response of our apparatus was calibrated using the melting enthalpy of Indium as a standard.

X-ray powder diffraction experiments were realized with the help of two kinds of apparatus. First, a Guinier-Lenné camera Enraf-Nonius, working in transmission, allows to point out the crystallographic changes versus temperature on the photographic diffraction pattern. The experimental conditions were as follows: heating (or cooling) rates of $0.1\,K\,min^{-1}$; Cu K$\alpha$ radiation, quartz monochromator; powder sample maintained between two thin aluminium sheets (12 μ) for a proper repartition of the temperature on the whole diffracting surface of the sample. In a second time, in order to get accurate values of the $\theta$ (Bragg angle) positions of the diffraction lines, a powder Siemens D500 diffractometer equipped with a heating TTK-Anton Paar unit was used. The position of the diffraction lines was estimated with an accuracy of $\pm 0.01°$ ($\theta$). Such a precision was estimated to be necessary for further attempts to determine the crystallographic data (unit-cell parameters) of the different polymorphic phases of $C_{12}Zn$ and $C_{10}Zn$. With this purpose, we used the last version of DICVOL program (DICVOL91[13] which is an improved version of the first DICVOL72),[14] a powerful automatic indexing method of powder diffraction patterns. First attempts with DICVOL91 program were made using 20 experimental diffraction lines and the solutions were then refined with more diffraction lines, using the AFMAIL program of our laboratory.

Samples for the infrared measurements were obtained by rapid evaporation of an ethanolic solution on a CsI window. The spectrometer was a Bruker 113 V interferometer equipped with a MCT detector. The resolution was $2\,cm^{-1}$ and 200 scans were accumulated. The samples were inside a home-built evacuated chamber[15] where temperatures were stable within 1°C.

Raman spectra of powdered samples were recorded on a Coderg T800 spectrometer equipped with a triple monochromator. Sample temperatures were regulated by means of a Coderg CRN2 continuous nitrogen flow cryostat and fluctuated less than 1°C. The spectral slit width was about 2.5cm$^{-1}$. The 514.5 or 488 nm lines of a Spectra Physics Ar ion laser model 171 were used for excitation, with a power varying from 50 to 150 mW depending on the spectral domain.

## II. RESULTS

### II.1 Differential Scanning Calorimetry

The DSC curves observed during heating and cooling processes are presented in Figures 2 and 3 for $C_{10}Zn$ and $C_{10}Zn$ respectively. In the 293–453 K range, two phase transitions at temperature $T^1$ and $T^2$ are observed for both compounds; they define the domains of three phases named RTP, MTP and HTP. The results are in good agreement with those published by Socias *et al.*,[11] but some small differences could be pointed out concerning the numerical values. They are likely explained by the higher rates of temperature variations (8 K min$^{-1}$) used by the authors. Tables I and II present the characteristic features of the DSC signals for $C_{12}Zn$ and $C_{10}Zn$ respectively.

Some remarks need to be made. The first phase transition RTP↔MTP is very energetic (40.9 KJ mole$^{-1}$ for $C_{10}Zn$ and 54.9 KJ mole$^{-1}$ for $C_{12}Zn$) compared with the second phase transition MTP↔HTP (8.3 KJ mole$^{-1}$ for $C_{10}Zn$ and 7.1 KJ mole$^{-1}$ for $C_{12}Zn$). All the transitions can be considered as of first order as it can be deduced from the existence of some thermal hysteresis on the cooling DSC values. The delay is

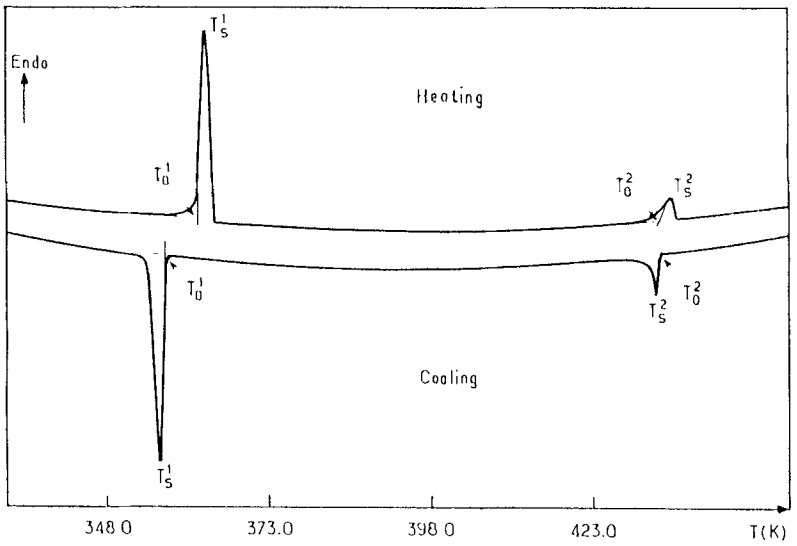


FIGURE 2 DSC heating and cooling curves obtained for $C_{12}Zn$.

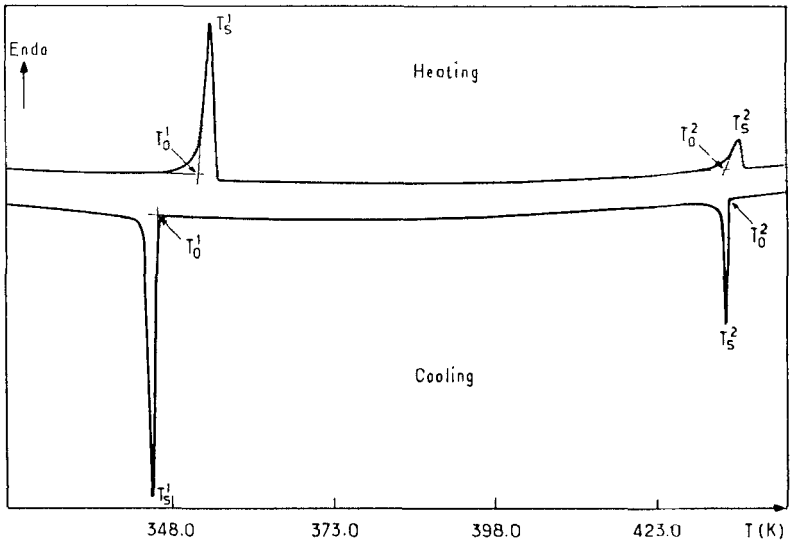


FIGURE 3 DSC heating and cooling curves obtained for $C_{10}Zn$.

TABLE I

DSC signals observed in $C_{12}Zn$ (2K $min^{-1}$).

| | RTP↔MTP transition | | | MTP↔HTP transition | | |
|---|---|---|---|---|---|---|
| Scanning process | $T_o^1$(K) | $T_s^1$(K) | ΔH (KJ $mole^{-1}$) | $T_o^2$(K) | $T_s^2$(K) | ΔH (KJ $mole^{-1}$) |
| Heating | 362.4 | 363.6 | 54.9 ± 0.1 | 433.0 | 435.0 | 7.1 ± 0.2 |
| Cooling | 358.8 | 357.2 | | 433.0 | 432.5 | |

TABLE II

DSC signals observed in $C_{10}Zn$ (2K $min^{-1}$).

| | RTP↔MTP transition | | | MTP↔HTP transition | | |
|---|---|---|---|---|---|---|
| Scanning process | $T_o^1$(K) | $T_s^1$(K) | ΔH (KJ $mole^{-1}$) | $T_o^2$(K) | $T_s^2$(K) | ΔH (KJ $mole^{-1}$) |
| Heating | 352.6 | 354.7 | 40.9 ± 0.5 | 433.6 | 435.9 | 8.3 ± 0.2 |
| Cooling | 349.1 | 347.8 | | 433.0 | 432.5 | |

more important for the first phase transition RTP↔MTP (3.5 K for $C_{10}Zn$ and 3.6 K for $C_{12}Zn$) than for the second one MTP↔HTP (0.6 K for $C_{10}Zn$ and 0.0 K for $C_{12}Zn$). The comparison of the transition enthalpies $\Delta H^1$ and $\Delta H^2$ shows that the main structural changes are observed at the RTP↔MTP transition for both compounds. This result will be confirmed by preliminary X-ray diffraction studies.

## II.2 Differaction results

### *II.2.1. Guinier-Lenné investigation*

The X-ray diffraction experiment performed on $C_{12}Zn$ in the temperature range 293 K–453 K (Figure 4) shows the presence of two phase transitions, near 360 K and 430 K. These results are in agreement with the calorimetric data. Important crystallographic changes are observed at these temperatures: those which occur at the first transition, corresponding to the RTP↔MTP phase change, present the following characteristics:

—presence of numerous sharp diffraction lines in the two phases, showing the existence of an ordered structural organization in both structures.

—a strong and abrupt modification of the interlayer distance $d_{001}$ (identified by the shift of the first diffraction lines situated on the left of the pattern (Figure 4): for example, $d_{002}^{RTP} = 21.3$ Å in the RTP phase becomes $d_{002}^{MTP} = 25.6$ Å in the MTP phase, i.e. an increase of about 20%. Let us recall that this value corresponds to the distance between two successive mineral layers $(ZnCl_4)^{--}$ in the direction roughly parallel to the length of the organic chains $(CH_3\text{-}(CH_2)_{11}\text{-}NH_3)^+$.

For the HTP form, the Guinier-Lenné pattern shows the disappearance of almost all the diffraction lines. This is an indication of a high degree of disorder in this structure. The only observed diffraction lines are those corresponding to the $d_{001}$ distance, which is slightly increased: the $d_{004}^{HTP}$ distance equal to 13.5 Å corresponds to a rise of about 3% with respect to the distance in the MTP phase. The presence of the $d_{001}$ lines in the HTP phase shows that the structure still keeps a two-dimensional character, but the ordered crystallographic organization of the molecular part between two successive mineral layers has been entirely destroyed. At still higher temperatures, the $d_{001}$ lines disappear, which indicate the loss of any ordered arrangement.

Guinier-Lenné diffraction results obtained by heating polycrystalline $C_{10}Zn$ from 293 K to 363 K are given in Figure 5. The phase transition RTP↔MTP near 350 K is

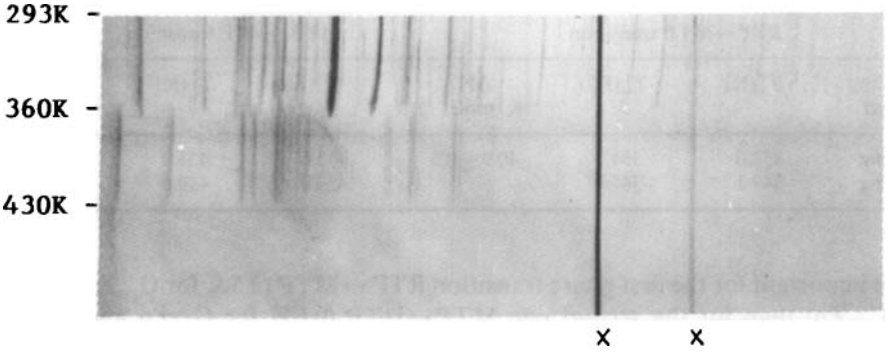


FIGURE 4 Phase transitions in $C_{12}Zn$ observed by Guinier-Lenné experiment (the lines marked (*X*) correspond to the sample holder).

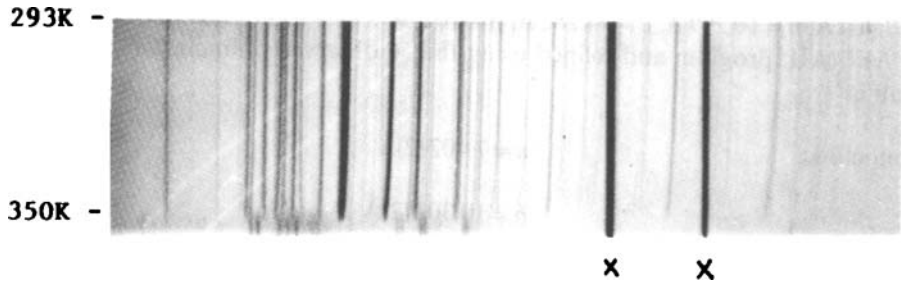


FIGURE 5 Phase transition in $C_{10}Zn$ observed by Guinier-Lenné experiment (the lines marked (*X*) correspond to the sample holder).

evidenced by an obvious change of the structural organization. Both forms keep a well-ordered structure characterized by the presence of numerous sharp diffraction lines. This thermal behaviour of $C_{10}Zn$ is similar to that observed previously for the $C_{12}Zn$ compound. A strong increase of the interlayer distance is also observed during the RTP↔MTP phase transition: for example, $d_{002}^{RTP}$ equal to 18.6 Å becomes $d_{002}^{MTP} = 22.1$ Å in the MTP phase which corresponds to a 19% rise, quite similar to the percentage observed in $C_{12}Zn$. As the Guinier-Lenné diagrams show a similar behaviour of $C_{10}Zn$ and $C_{12}Zn$ as a function of temperature, we did not study the HTP phase of the $C_{10}$ compound; indeed the cations were shown to be quite disordered in the $C_{12}Zn$ HTP phase. Therefore, we shall consider only the two phases RTP and MTP in the following study.

### *II.2.2. Search for crystallographic parameters of RTP and MTP phases*

#### *II.2.2.1 $C_{12}Zn$*

*RTP phase:* The application of the DICVOL91 program to the first 24 lines of the powder pattern (Figure 6) leads to the following solution: monoclinic system,

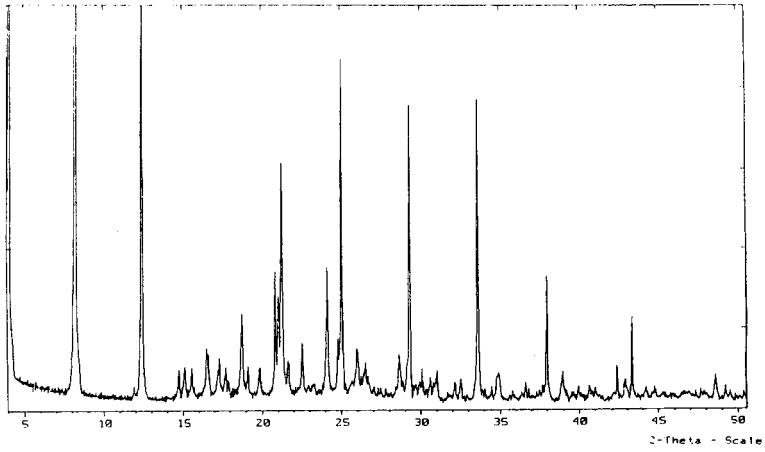


FIGURE 6 Powder diffraction diagram of $C_{12}Zn$ (RTP phase).

$a = 7.404$ Å, $b = 10.299$ Å, $c = 44.282$ Å, $\beta = 105.68°$. This solution is then introduced in the AFMAIL program and refined using the 56 observed diffraction lines. The final result is:

Monoclinic, $a = 7.402(2)$Å

$b = 10.302(2)$Å

$c = 44.262(8)$Å

$\beta = 105.65(3)°$

The differences between observed and calculated values are given in Table III. They are less than 0.02°. Our results are in good agreement with those obtained by Ciajolo *et al.*[1] from a single crystal study: $a = 7.409(3)$Å, $b = 10.379(5)$Å, $c = 44.399(10)$Å, $\beta = 105.56(5)°$, space group $P2_1/c$, $Z = 4$.

*MTP phase:* The powder diffraction diagram, realized at 370 K, presents a small number of diffraction lines. About 20 lines have been retained for the unit-cell-parameters search. DICVOL91 and AFMAIL programs were used for this determination and the solution corresponding to the best figure of merit of DICVOL91 program is:

Monoclinic, $a = 5.940(2)$Å

$b = 10.631(4)$Å

$c = 52.479(17)$Å

$\beta = 102.18(2)°$

The differences between observed and calculated $\theta$ values given in Table IV are less than 0.02°. The hkl indices of diffraction lines are compatible with space group $P2_1/m$ or P2/m. This solution obtained from a poor powder diffraction diagram must be considered with usual reservations. Nevertheless, the distance between two successive mineral layers $d_{002}^{MTP} = c/2 \sin\beta = 25.65$ Å evidences an actual strong increase with respect to the distance in the RTP phase ($d_{002}^{RTP} = 21.31$ Å).

### *II.2.2.2* $C_{10}Zn$

*RTP phase:* The same procedure was followed to obtain an accurate diffraction diagram of the room temperature phase of $C_{10}Zn$ (Figure 7). Using the DICVOL91 program leads to a unique solution, from the first 20 diffraction lines: monoclinic, $a = 7.376$ Å, $b = 10.356$ Å, $c = 39.099$ Å, $\beta = 106.16°$. The three parameters $\vec{a}$, $\vec{b}$ and $\beta$ show many similarities with those of the RTP unit-cell of $C_{12}Zn$. This solution has

TABLE III

Diffraction data of $C_{12}Zn$ (RTP phase).

| $h$ | $k$ | $l$ | $\theta_{obs}(°)$ | $\theta_{cal}(°)$ | $\Delta\theta(°)$ |
|---|---|---|---|---|---|
| 0 | 0 | 2 | 2.064 | 2.071 | −0.007 |
| 0 | 0 | 4 | 4.136 | 4.146 | −0.010 |
| 0 | 1 | 4 | 5.955 | 5.970 | −0.015 |
| 0 | 0 | 6 | 6.214 | 6.225 | −0.011 |
| −1 | 1 | 2 | 7.367 | 7.373 | −0.006 |
| 1 | 1 | 0 | 7.548 | 7.551 | −0.003 |
| −1 | 1 | 4 | 7.773 | 7.770 | 0.003 |
| 1 | 1 | 2 | 8.274 | 8.269 | 0.005 |
| −1 | 1 | 6 | 8.653 | 8.667 | −0.014 |
| 0 | 2 | 2 | 8.851 | 8.850 | 0.001 |
| −1 | 0 | 8 | 8.954 | 8.941 | 0.013 |
| 0 | 1 | 8 | 9.367 | 9.368 | −0.001 |
| 0 | 2 | 4 | 9.558 | 9.561 | −0.003 |
| −1 | 1 | 8 | 9.925 | 9.931 | −0.006 |
| 0 | 0 | 10 | 10.415 | 10.412 | 0.003 |
| −1 | 1 | 2 | 10.499 | 10.505 | −0.006 |
| 1 | 2 | 0 | 10.624 | 10.632 | −0.008 |
| 1 | 1 | 6 | 10.821 | 10.837 | −0.016 |
| 0 | 1 | 10 | 11.277 | 11.279 | −0.002 |
| −1 | 2 | 6 | 11.463 | 11.461 | 0.002 |
| 1 | 1 | 7 | 11.636 | 11.631 | 0.005 |
| −2 | 0 | 2 | 12.072 | 12.081 | −0.009 |
| −1 | 0 | 12 | 12.404 | 12.394 | 0.010 |
| 0 | 0 | 12 | 12.514 | 12.525 | −0.011 |
| −2 | 1 | 4 | 12.816 | 12.802 | 0.014 |
| −2 | 1 | 1 | 13.001 | 12.989 | 0.012 |
| 2 | 1 | 0 | 13.237 | 13.220 | 0.017 |
| 2 | 1 | 1 | 13.515 | 13.530 | −0.015 |
| −1 | 2 | 10 | 13.715 | 13.709 | 0.006 |
| 2 | 1 | 2 | 13.898 | 13.914 | −0.016 |
| −1 | 3 | 2 | 14.317 | 14.322 | −0.005 |
| 0 | 0 | 14 | 14.658 | 14.656 | 0.002 |
| 1 | 3 | 2 | 14.807 | 14.818 | −0.011 |
| −2 | 2 | 1 | 15.042 | 15.035 | 0.007 |
| 0 | 1 | 14 | 15.290 | 15.298 | −0.008 |
| 1 | 3 | 4 | 15.502 | 15.502 | 0.000 |
| 2 | 2 | 2 | 15.864 | 15.850 | 0.014 |
| 2 | 1 | 6 | 16.080 | 16.078 | 0.002 |
| −1 | 0 | 16 | 16.267 | 16.264 | 0.001 |
| 1 | 3 | 6 | 16.451 | 16.438 | 0.003 |
| 0 | 0 | 16 | 16.814 | 16.808 | 0.006 |
| 2 | 2 | 5 | 17.227 | 17.233 | −0.006 |
| 0 | 4 | 1 | 17.448 | 17.436 | 0.012 |
| −2 | 3 | 5 | 17.901 | 17.918 | −0.017 |
| 0 | 3 | 12 | 18.194 | 18.181 | 0.007 |
| −1 | 0 | 18 | 18.302 | 18.295 | 0.007 |
| 0 | 0 | 18 | 18.992 | 18.984 | 0.008 |
| −1 | 3 | 14 | 19.479 | 19.485 | −0.016 |
| 1 | 4 | 5 | 19.800 | 19.784 | 0.016 |
| 0 | 2 | 17 | 19.983 | 19.980 | 0.003 |
| −1 | 2 | 18 | 20.331 | 20.347 | −0.016 |
| 2 | 2 | 10 | 20.515 | 20.514 | 0.001 |
| 1 | 1 | 7 | 21.097 | 21.098 | −0.001 |
| 0 | 0 | 20 | 21.191 | 21.189 | 0.002 |
| −2 | 4 | 5 | 21.444 | 21.456 | −0.012 |
| 0 | 1 | 20 | 21.659 | 21.660 | −0.001 |

TABLE IV

Diffraction data of $C_{12}Zn$ (MTP phase, $T = 370$ K).

| $h$ | $k$ | $l$ | $\theta_{obs}(^\circ)$ | $\theta_{cal}(^\circ)$ | $\Delta\theta(^\circ)$ |
|---|---|---|---|---|---|
| 0 | 0 | 2 | 1.723 | 1.721 | 0.002 |
| 0 | 0 | 4 | 3.439 | 3.443 | −0.004 |
| 0 | 0 | 6 | 5.167 | 5.169 | −0.002 |
| 0 | 0 | 8 | 6.910 | 6.899 | 0.010 |
| −1 | 0 | 2 | 7.449 | 7.452 | −0.003 |
| 1 | 0 | 1 | 7.859 | 7.853 | 0.006 |
| 1 | 0 | 2 | 8.166 | 8.168 | −0.002 |
| −1 | 1 | 3 | 8.598 | 8.599 | −0.001 |
| −1 | 1 | 6 | 9.279 | 9.265 | 0.013 |
| 0 | 1 | 10 | 9.602 | 9.597 | 0.004 |
| 1 | 0 | 6 | 10.101 | 10.101 | 0.000 |
| 0 | 2 | 8 | 10.858 | 10.850 | 0.000 |
| 0 | 2 | 9 | 11.436 | 11.429 | 0.006 |
| −1 | 0 | 13 | 12.200 | 12.217 | −0.017 |
| 0 | 3 | 4 | 13.030 | 13.034 | −0.004 |
| 1 | 1 | 10 | 13.407 | 13.413 | −0.006 |
| −1 | 0 | 16 | 14.406 | 14.403 | 0.003 |
| 1 | 3 | 0 | 14.752 | 14.754 | −0.002 |
| −2 | 2 | 18 | 21.486 | 21.486 | −0.003 |
| −2 | 2 | 19 | 22.048 | 22.043 | 0.005 |

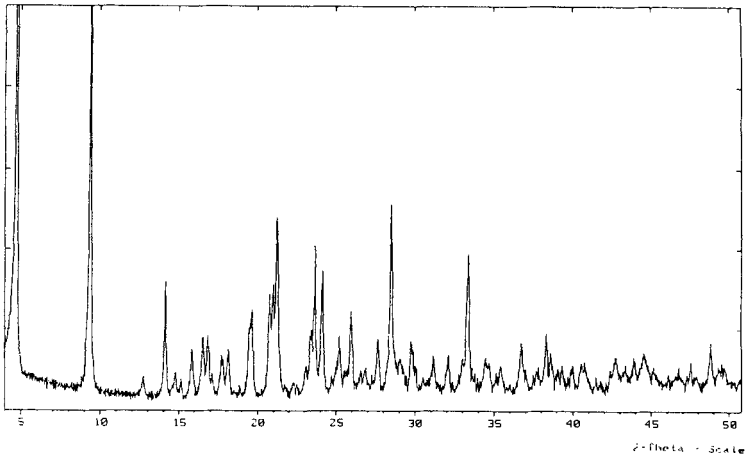


FIGURE 7 Powder diffraction diagram of $C_{10}Zn$ (RTP phase).

been applied to the whole diffraction diagram (38 observed lines) and the final solution obtained with AFMAIL program is:

Monoclinic, $a = 7.387(2)$Å

$b = 10.349(4)$Å

$$c = 39.084(12)\text{Å}$$

$$\beta = 106.11(4)^\circ$$

The differences between observed and calculated angles given in Table V are lower than 0.02° which strengthens the validity of this solution. The indices of diffraction lines are compatible with the space group $P2_1/c$, $Z=4$, so that this phase could be isomorphous with the RTP phase of $C_{12}Zn$. The distance between two successive mineral layers $d_{002}^{RTP} = c/2 \sin\beta = 18.77$ Å is 2.54 Å smaller than the distance in $C_{12}Zn$ (21.31 Å) which very well corresponds to the difference in length of $(C_{10}H_{21}NH_3)^+$ and

TABLE V

Diffraction data of $C_{10}Zn$ (RTP phase).

| $h$ | $k$ | $l$ | $\theta_{obs}(^\circ)$ | $\theta_{cal}(^\circ)$ | $\Delta\theta(^\circ)$ |
|---|---|---|---|---|---|
| 0 | 0 | 2 | 2.355 | 2.351 | 0.004 |
| 0 | 0 | 4 | 4.702 | 4.707 | −0.005 |
| 0 | 1 | 4 | 6.356 | 6.361 | −0.005 |
| 0 | 0 | 6 | 7.055 | 7.070 | −0.015 |
| −1 | 1 | 1 | 7.369 | 7.382 | −0.013 |
| 1 | 1 | 0 | 7.565 | 7.563 | 0.002 |
| 1 | 1 | 1 | 7.923 | 7.918 | 0.004 |
| 0 | 1 | 6 | 8.267 | 8.270 | −0.003 |
| 1 | 1 | 2 | 8.429 | 8.427 | 0.002 |
| 0 | 2 | 2 | 8.869 | 8.883 | −0.014 |
| 1 | 1 | 3 | 9.074 | 9.064 | 0.010 |
| 0 | 2 | 5 | 10.420 | 10.415 | 0.004 |
| 1 | 2 | 0 | 10.616 | 10.616 | 0.000 |
| 0 | 2 | 6 | 11.140 | 11.137 | 0.002 |
| 1 | 1 | 6 | 11.540 | 11.521 | 0.019 |
| 1 | 2 | 3 | 11.730 | 11.746 | −0.016 |
| 0 | 0 | 10 | 11.834 | 11.838 | −0.004 |
| −2 | 0 | 2 | 12.076 | 12.089 | 0.014 |
| −2 | 0 | 6 | 12.593 | 12.581 | 0.011 |
| 1 | 2 | 5 | 12.987 | 13.005 | 0.018 |
| 2 | 1 | 0 | 13.265 | 13.267 | −0.002 |
| 0 | 3 | 3 | 13.406 | 13.393 | 0.013 |
| −1 | 2 | 9 | 13.820 | 13.801 | 0.018 |
| 0 | 0 | 12 | 14.251 | 14.251 | 0.000 |
| −1 | 1 | 12 | 14.536 | 14.547 | −0.011 |
| 0 | 1 | 12 | 14.899 | 14.903 | −0.004 |
| 2 | 2 | 1 | 15.591 | 15.584 | 0.006 |
| −2 | 2 | 8 | 16.045 | 16.051 | −0.005 |
| 0 | 0 | 14 | 16.684 | 16.691 | −0.007 |
| 0 | 4 | 0 | 17.316 | 17.322 | −0.006 |
| 0 | 4 | 3 | 17.697 | 17.700 | −0.003 |
| 1 | 2 | −14 | 18.371 | 18.351 | 0.019 |
| 1 | 1 | 13 | 18.874 | 18.861 | 0.013 |
| 0 | 0 | 16 | 19.160 | 19.161 | −0.001 |
| 1 | 2 | 12 | 19.318 | 19.313 | 0.005 |
| 0 | 1 | 16 | 19.656 | 19.668 | −0.012 |
| 3 | 1 | −10 | 19.974 | 19.965 | 0.009 |
| 3 | 2 | −3 | 20.341 | 20.344 | −0.003 |

$(C_{12}H_{25}NH_3)^+$ ions in all-trans configuration, due to the presence of two additional methylene groups.

*MTP phase:* As already observed for the $C_{12}Zn$ derivative, the diffraction diagram corresponding to the MTP phase (measured at 356 K) only presents a few diffraction lines. About 20 observed lines are retained for the unit-cell parameters research. The final solution issued from DICVOL91 and AFMAIL programs is:

Monoclinic, $a = 6.218(6)$Å

$b = 9.374(6)$Å

$c = 45.433(33)$Å

$\beta = 103.00(10)°$

The differences between observed and calculated $\theta$ angles given in Table VI, are lower than 0.02°. Nevertheless, the low number of observed diffraction lines leads to consideration of this solution with usual reserves, though the order of magnitude of the parameters $a$, $b$ and $\beta$ is about the same as in the MTP unit-cell of $C_{12}Zn$. The distance between two successive mineral layers in this structure $d_{002}^{MTP} = 22.13$ Å is larger than in the RTP phase (18.77 Å) which confirms the strong abrupt increase (+3.36 Å) accompanying the transition RTP → MTP.

TABLE VI

Diffraction data of $C_{10}Zn$ (MTP phase).

| $h$ | $k$ | $l$ | $\theta_{obs}(°)$ | $\theta_{cal}(°)$ | $\Delta\theta(°)$ |
|---|---|---|---|---|---|
| 0 | 0 | 2 | 1.991 | 1.994 | −0.003 |
| 0 | 0 | 4 | 3.985 | 3.991 | −0.006 |
| 0 | 0 | 6 | 5.992 | 5.992 | 0.000 |
| −1 | 0 | 4 | 7.489 | 7.498 | −0.009 |
| 0 | 1 | 6 | 7.617 | 7.635 | −0.018 |
| −1 | 0 | 6 | 8.347 | 8.351 | −0.004 |
| −1 | 1 | 1 | 8.587 | 8.574 | 0.014 |
| 1 | 1 | 1 | 8.937 | 8.953 | −0.016 |
| 1 | 1 | 2 | 9.297 | 9.300 | −0.003 |
| 0 | 2 | 0 | 9.443 | 9.459 | −0.016 |
| 0 | 2 | 2 | 9.682 | 9.671 | 0.011 |
| 0 | 0 | 10 | 10.038 | 10.021 | 0.017 |
| 0 | 2 | 5 | 10.720 | 10.717 | 0.003 |
| 0 | 1 | 10 | 11.091 | 11.095 | −0.004 |
| 0 | 0 | 12 | 12.059 | 12.052 | 0.006 |
| 1 | 2 | 1 | 12.190 | 12.174 | 0.015 |
| −1 | 2 | 5 | 12.369 | 12.353 | 0.016 |
| −1 | 2 | 7 | 13.047 | 13.057 | −0.010 |
| 0 | 2 | 9 | 13.121 | 13.121 | 0.000 |
| 1 | 2 | 5 | 13.646 | 13.654 | −0.008 |

## II.3 Spectroscopic analysis

In this section, attention will be drawn to the spectral features which can bring clear information on the structural changes occuring in the chain conformation or in the intermolecular couplings. Only the RTP and MTP phases are studied. Figures 8–10 display the evolution of the infrared and the Raman spectra in the main domains which are relevant to our analysis.

### $C_{12}Zn$

The factor group of $C_{12}Zn$ is isomorphic to the point group $C_{2h}$ (2/m) and the unit-cell contains four molecules.[1] As the symmetry of the site is $C_1$ (1), each molecular vibration gives rise to one component in each symmetry species of the factor group, $A_g$, $B_g$, $A_u$ and $B_u$. The $A_g$ and $B_g$ components are only Raman active, while the $A_u$ and $B_u$ components are only infrared active. According to X-ray results, the dodecyl ammonium chains are in all-trans conformation.

The infrared spectrum indeed shows progression bands due to intramolecular coupling of adjacent oscillators in a planar extended ordered structure (Figure 8) and the most intense bands in the Raman spectrum are those of all-trans forms. The spectral domain corresponding to the CH stretching looks like that of solid *n*-paraffins (Figure

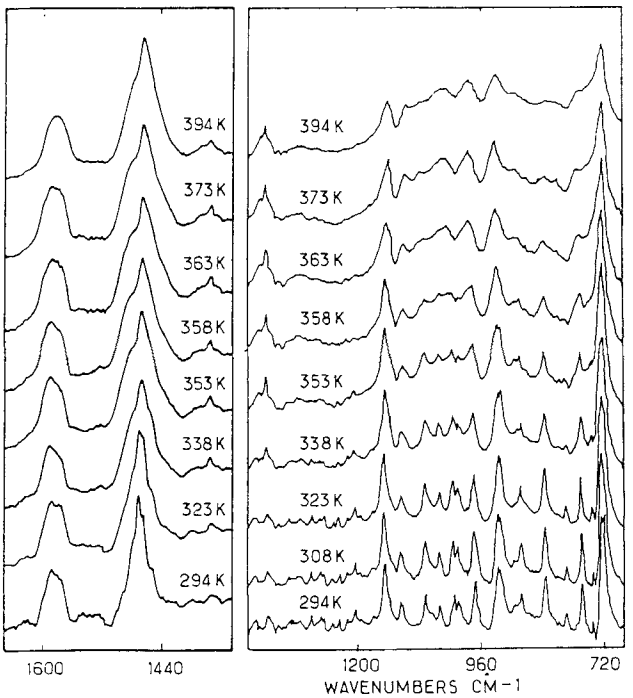


FIGURE 8 Temperature effect on the IR spectra of $C_{12}Zn$.

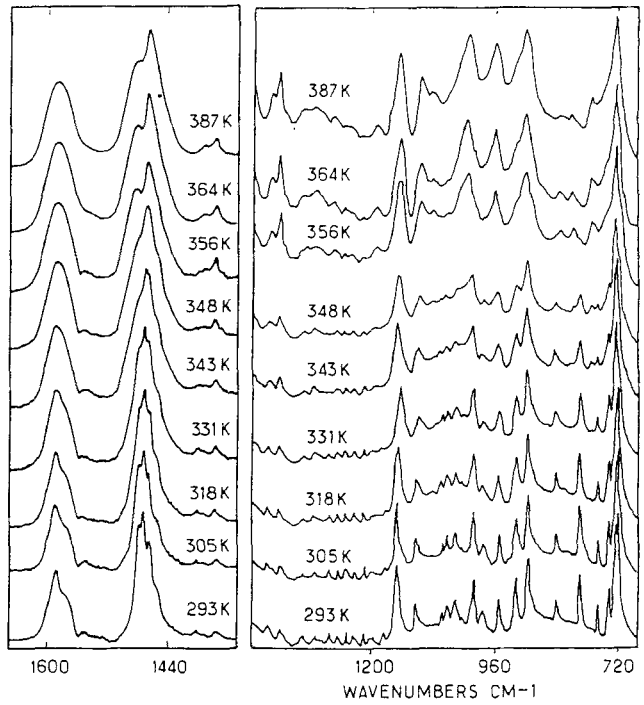


FIGURE 9 Temperature effect on the IR spectra of $C_{10}Zn$.

10).[16] It presents well-defined peaks corresponding to fundamental vibrations of the $CH_2$ and $CH_3$ groups and broad features which are due to Fermi resonances between the fundamentals and the quasi-continuum of the bending progression band overtones. The frequency of the longitudinal acoustic mode (LAM) characteristic of the length of extended chains is 186 $cm^{-1}$. It is higher than in corresponding *n*-alkane[17] which is consistent with the value expected for all-trans chains engaged in hydrogen bonds. When raising the temperature, the progression bands broaden and tend to disappear at about 338 K. But no absorption corresponding to specific bond sequences is observed with a noticeable intensity. On the other hand, the LAM line is still present at the same frequency at 333 and 353 K. It thus seems that the chains are mainly in extended conformation within the whole domain of the RTP phase. At 368 K, the characteristic bands of extended chains are no longer present in the Raman spectrum and the group of bands between 2880 and 2940 $cm^{-1}$ assigned to Fermi resonances between the symmetric $CH_2$ stretching and overtones of the methylene bending vibrations of gauche forms strongly broadens (Figure 10) and the LAM mode is not observed. In the infrared spectrum (Figure 8), the progression bands have disappeared from the whole spectrum and new features, such as a broad absorption near 1310 $cm^{-1}$ and a weak one at about 1340 $cm^{-1}$ are observed and a shoulder at 1367 $cm^{-1}$ and a weak band near 1354 $cm^{-1}$, which persist in the spectrum while bands of the extended chains have vanished, are due to specific defects. The signals at 1340 and 1354 $cm^{-1}$ are characteris-

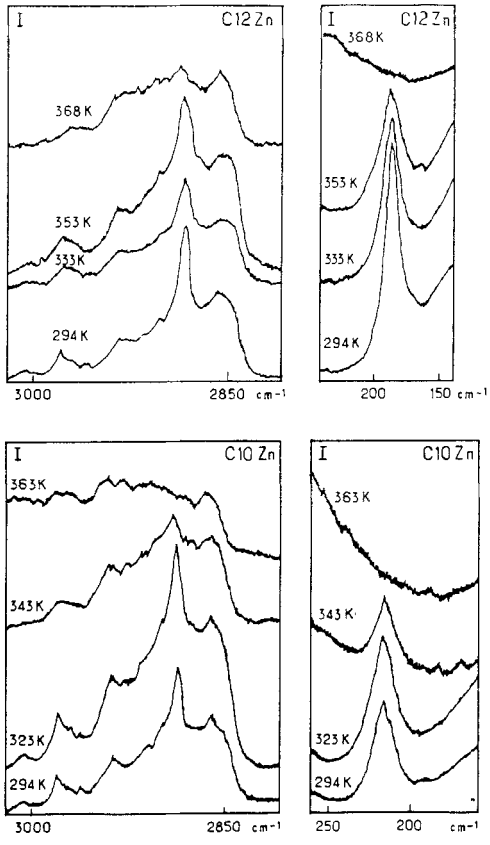


FIGURE 10 Raman spectra of $C_{12}Zn$ and $C_{10}Zn$ versus temperature.

tic of some end gauche forms and a few *gg* sequences respectively; those at 1310 and 1367 $cm^{-1}$ indicate the presence of defects of the form $gt^{2n-1}g$ or $gt^{2n-1}g'$.[5,18,19] As the area of ionic layer per metal atom does not increase at the transition step,[3] $gt^{2n-1}g$ forms are probably excluded.

At room temperature, the $\delta_s(CH_3)$ frequency is 1378 $cm^{-1}$, which is higher than the value in $C_{10}Cd$ for instance, 1375 $cm^{-1}$.[5] The frequency is unchanged in the high temperature phase. It is about the same as the value found in disordered phases of layer perovskites. This indicates that the interactions between the methyl extremities are weaker and can be related to the different packing of the chains: as they are interdigitated, the $CH_3$ ends do not face each other as in Cd, Mn, or Cu compounds, which has already been emphasized in the case of $C_{14}Zn$.[20]

The $r(CH_2)$ splitting (718–723 $cm^{-1}$) progressively diminishes above 308 K as the frequency of the lower component increases and this feature disappears at 353 K. At 363 K the band shape changes and appears characteristic of molten *n*-alkanes. The $\delta(CH_2)$ splitting on the infrared spectrum (1446–1473 $cm^{-1}$) also decreases with increasing temperature and it disappears at 338 K. No splitting of the $CH_2$ bending is

observed on the Raman spectrum at room temperature, however the symmetrical component of this splitting appears at 1434 $cm^{-1}$ at liquid nitrogen temperature. This frequency is higher than the value in $C_{10}Cd$ (1424 $cm^{-1}$),[5] which suggests that the intermolecular interactions are weaker.

The phase change of $C_{12}Zn$ is thus related to the abrupt occurence of an important conformational disorder since the hydrocarbon parts suddenly lose the characteristic features of extended chains. Kinks of the form $gt^{2n-1}g'$ are the main defects observed in the MTP phase. The cation mobility is important within the RTP phase which is consistent with weak intermolecular interactions.

### $C_{10}Zn$

The space group of crystalline $C_{10}Zn$ (RTP phase) is likely $P2_1/c$ with four molecules in the unit-cell. Thus, two of the four components of each molecular vibration are active in Raman and the other two in IR. The conformation of the hydrocarbon part is not known but it can be deduced from vibrational spectrum analysis. Features characteristic of extended chains are observed in the Raman spectrum in the 1000–1200 $cm^{-1}$ range, as well as in the $\nu$(CH) and $\delta$(CH) spectral domains. The infrared spectrum at room temperature shows well-defined progression bands (Figure 9). Their frequencies are in rather good agreement with the values for an all-trans decylammonium cation calculated using a normal coordinate treatment and observed in the spectrum of $C_{10}Cl$ $\varepsilon$ phase.[10] The Raman frequency of the longitudinal acoustic mode (LAM), 215 $cm^{-1}$, is the same as for $C_{10}Cl$ ordered phases which contain all-trans chains engaged in hydrogen bonds.[10]

When raising the temperature, the progression bands broaden at 348 K and abruptly disappear between 348 and 356 K. At 356 K, the kink absorption at 1308 $cm^{-1}$ is important but the 1367 $cm^{-1}$ feature is hardly visible as a shoulder at the bottom of the intense $\delta_s(CH_3)$ band. Some end gauche bonds near the methyl end are evidenced by the band near 1335 $cm^{-1}$ while a few *gg* sequences probably are responsible for the very weak maximum near 1353 $cm^{-1}$.[5] The Raman spectrum also displays characteristic features of extended chains which are lost at the phase transition and the LAM mode is not observed in the MTP phase.

At room temperature, the $\delta_s(CH_3)$ absorption at 1378 $cm^{-1}$ is shifted upwards by only 1 $cm^{-1}$ in the high temperature phase. Factor group splittings are observed on $r(CH_2)$ (718–724 $cm^{-1}$), $\delta(CH_2)$ (1466—1473 $cm^{-1}$) and $\nu_a(CH_2)$ (2919–2929 $cm^{-1}$) absorption bands. As in $C_{10}Zn$, splitting of the $CH_2$ bending is observed in the Raman spectrum at 1435 $cm^{-1}$ at liquid nitrogen temperature but not at room temperature. The $NH_3$ group frequencies, stretching, symmetrical and antisymmetrical deformations, are about the same in both $C_{10}$ and $C_{12}$ derivatives, which indicates that the environment of the polar heads and the strength of hydrogen bonds are similar. With increasing temperature, the factor group splitting of $r(CH_2)$ progressively diminishes and is lost at 331 K. The distance between the two components of $\delta(CH_2)$ diminishes and they overlap at the transition at the same time as the $\nu_a(CH_2)$ components.

Therefore this analysis results in a picture of the room temperature phase of $C_{10}Zn$ as an ordered solid which presents intramolecular coupling in all-trans chains. Some bands are split into two components, due to intermolecular coupling and this is

consistent with the existence of at least two molecules in the unit-cell. The disordering process also resembles that of the $C_{12}$ compound though the cation mobility in the RTP phase seems lower.

## III. CONCLUSION

The combined results of X-ray diffraction and vibrational spectroscopy experiments lead to a description of the various structures and disordering processes of $C_{12}Zn$ and $C_{10}Zn$ crystals.

1. The room temperature phase of $C_{10}Zn$ is a well-ordered three periodic structure. The structural arrangement looks similar to that of $C_{12}Zn$. The alkylammonium chains are in the all trans-conformation. They are interdigitated and the packing is loose since the intermolecular coupling is small. As the analysis of the spectra shows a great similarity of the $NH_3$ surroundings in $C_{10}Zn$ and $C_{12}Zn$, the binding of the chains to the ionic layers and the structure of the inorganic sheets are probably similar.

   Within the series $(C_nH_{2n+1}NH_3)_2\ ZnCl_4$, the variation of the interlayer distance with the number of carbon atoms $d_{001}$ $(n)$, is linear (Figure 11). This is true for the MTP as for the RTP forms and is consistent with similar structures and cation conformations in the different phases of the compounds.
2. The spectra show an important modification of the structure of the organic part when raising the temperature within the RTP phase of $C_{12}Zn$. Inter and intramolecular couplings are lost and broad absorptions are observed at 338 K i.e. 26 K below the RTP↔MTP transition; they are likely related to an important mobility of the chains in this phase. But no specific defect is evidenced. If the

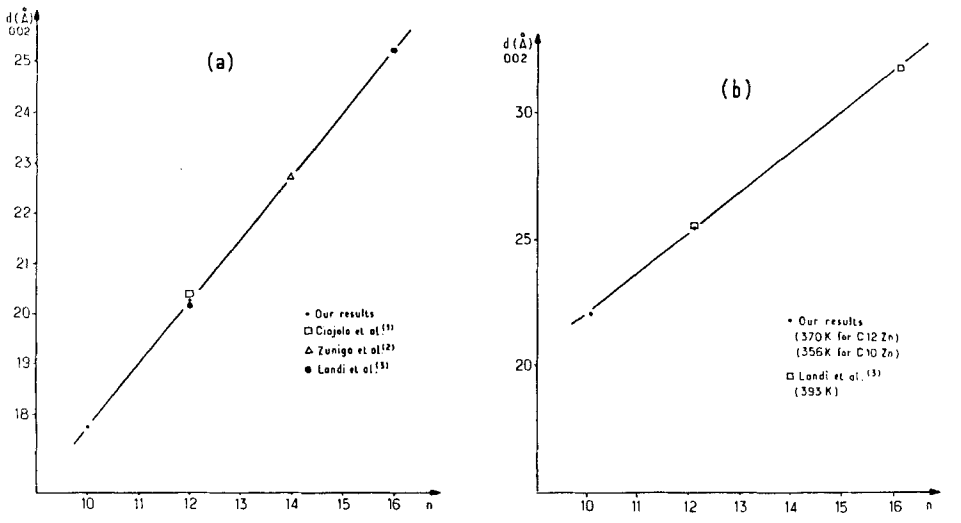


FIGURE 11 Variations of the interlayer distance in the series $(C_nH_{2n+1}NH_3)_2\ ZnCl_4$ versus the parameter n.a/RTP phase; b/MTP phase.

cations in extended form are described as parallel cylindrical rods, the occurrence of such sequences would increase their diameter, in a way which is not compatible with the RTP structure since the area per chain, 19 Å,$^2$ does not allow any gauche form. Then the chain disorder in this phase could be better described by rotational fluctuations of the chains, for instance cooperative torsion processes of the —$CH_2$— units along the chains may be coupled with overall molecular motions as observed, for instance, in the thermally activated disorder of the alkyl chains in other bidimensional compounds.[7]

Comparable cation behaviour is observed within the $\varepsilon$ phase of the *n*-alkyl ammonium chlorides ($C_8Cl$ and $C_{10}Cl$)[10,22] which presents entirely extended chains at liquid nitrogen temperature. When warming up inside phase $\varepsilon$, molecular interactions weaken, suggesting an increase of the chain mobility, and a few conformational defects of the kink form appear; this can be realized thanks to a relatively high area per chain of about 22 Å$^2$. The phenomenon is far less important in the RTP phase of the $C_{10}Zn$ compound, where a broadening of the progression bands is observed about 4 K below the RTP↔MTP transition. The difference of the chain mobility between the $C_{10}Zn$ and $C_{12}Zn$ compounds increases for $C_{14}Zn$: in the latter case, the chain disorder induced by the raising temperature in the RTP phase is sufficient to induce a weak modification in the unit-cell parameters corresponding to a small conformational change in the structure, before the order-disorder transition.[21]

3. The RTP↔MTP transition is characterized by an abrupt increase of the interlayer distance, about 20%. A similar increase has been observed at the ITP-HTP transition of $C_{14}Zn$.[21] A complete conformational disorder of the organic chains suddenly appears, at the same time as the changes in the unit cell parameters. At the transition, the area of the ionic layer per metal atom diminishes by about 17% in $C_{12}Zn$ and 23% in $C_{10}Zn$; this percentage is clearly larger than the decrease calculated for $C_{12}Zn$ (8,3%)[3] and $C_{14}Zn$ (10%)[21] which can be explained by the use of different techniques. Thus the appearance of new bond sequences such as kinks and end gauche forms implies a disinterdigitation of the chains to accommodate the increase of their diameter. This is a first order reconstructive transition. With the hypothesis of a complete disinterdigitation,[21] the observed increase of the interlayer distance is smaller than expected for all-trans chains facing each other. Indeed in such a case the interlayer distances would be superior to 30.36 Å for $C_{12}Zn$ and 25.30 Å for $C_{10}Zn$ while the experimental values are 25.65 Å and 22.13 Å respectively. The presence of kinks shortens the chain length (1.27 Å for one kink), then at least four or three kinks would be necessary to appear between the layers of $C_{12}Zn$ and $C_{10}Zn$ respectively. But the total reversibility of the phenomenon observed on the X-ray diffraction, calorimetric and spectroscopic diagrams suggests that the disinterdigitation is only partial, at least in the studied temperature domain.

## References

1. M. R. Ciajolo, P. Corradini and V. Pavone, *Acta Cryst.*, **B33**, 553 (1977).
2. F. J. Zuniga and G. Chapuis, *Cryst. Struct. Comm.* **10**, 533 (1981).

3. E. Landi, V. Salerno and M. Vacatello, *Gazz. Chim. Italiana*, **107**, 27 (1977).
4. R. Kind, S. Plesko, H. Arend, R. Blinc, B. Zeks, J. Seliger, B. Lozar, J. Slak, A. Levstik, G. Filipic, V. Zagar, G. Lahajnar, F. Milia and G. Chapuis, *J. Chem. Phys.*, **71**, 2118 (1979).
5. L. Ricard, M. Rey-Lafon and C. Biran, *J. Phys. Chem.*, **88**, 5614 (1984).
6. M. Vacatello and P. Corradini, *Gazz. Chim. Italiana*, **103**, 1027 (1973).
7. F. Guillaume, G. Coddens, A. J. Dianoux, W. Petry, M. Rey-Lafon and C. Sourisseau, *Mol. Phys.*, **67**, 665 (1989).
8. J. H. Choy, J. K. Kang, J. C. Park, N. B. Chanh and M. Rey-Lafon, *J. Chim. Phys. Fr.*, **90**, 1829 (1993).
9. N. B. Chanh, C. Lartigue-Bourdeau, M. Khechoubi, J. K. Kang, J. H. Choy and M. Rey-Lafon, *Mol. Cryst. Liq. Cryst.*, **238**, 93 (1994).
10. K. J. Shenk, C. A. Ogle, G. Chapuis, R. Cavagnat, A. Jokic and M. Rey-Lafon, *J. Phys. Chem.*, **93**, 5040 (1989).
11. C. Socias, M. A. Arriandiaga, M. J. Tello, J. Fernandez and P. Gili, *Phys. Stat. Sol.*, **57**, 405 (1980).
12. J. Fenrych, E. C. Reynhardt, S. Jurga and K. Jurga, *Mol. Phys.*, **78**, 1117 (1993).
13. A. Boutif and D. Louer, *J. App. Cryst.*, **24**, 987 (1991).
14. D. Louer and M. Louer, *J. App. Cryst.*, **5**, 271 (1972).
15. J. C. Cornut, P. V. Huong, A. Graja and Daleau *Appl. Spectrosc.*, **8**, 1401 (1988).
16. R. G. Snyder, S. L. Hsu and S. Krimm, *J. Chem. Phys.*, **72**, 5798 (1980).
17. J. R. Scherer and R. G. Snyder, *J. Phys: Chem.*, **72**, 5798 (1980).
18. L. Ricard, R. Cavagnat and M. Rey-Lafon, *J. Phys. Chem.*, **89**, 4887 (1985).
19. J. K. Kang, J. H. Choy and M. Rey-Lafon, *J. Phys. Chem. Solids*, **54**, 1567 (1993).
20. C. Almirante, G. Minoni and G. Zerbi, *J. Phys. Chem.*, **90**, 852 (1986).
21. J.Fernandez, C. Socias, M. A. Arriandiaga, M. J. Tello and A. Lopez Echarri, *J. Phys.*, C, **15**, 1151 (1982).
22. K. J. Schenk, C. A. Ogle, D. Schwarzenbach, G. Chapuis, J. C. Cornut and M. Rey-Lefon, *J. Phys. Chem.*, **96**, 5530 (1992).